Spatially resolved spectroscopic measurements of a dielectric barrier discharge plasma jet applicable for soft ionization

S.B. Olenici-Craciunescu [a], S. Müller [a], A. Michels [a], V. Horvatic [b], C. Vadla [b], J. Franzke [a],*

[a] ISAS–Leibniz Institut für analytische Wissenschaften, Otto-Hahn-Straße 6b, 44227 Dortmund, Germany
[b] Institute of Physics, Bijenicka 46, 10000 Zagreb, Croatia

ARTICLE INFO

ABSTRACT

An atmospheric pressure microplasma ionization source based on a dielectric barrier discharge with a helium plasma cone outside the electrode region has been developed for liquid chromatography/mass spectrometry and as ionization source for ion mobility spectrometry. It turned out that dielectric barrier discharge ionization could be regarded as a soft ionization technique characterized by only minor fragmentation similar to atmospheric pressure chemical ionization (APCI). Mainly protonated molecules were detected. In order to characterize the soft ionization mechanism spatially resolved optical emission spectrometry (OES) measurements were performed on plasma jets burning either in He or in Ar. Besides to spatial intensity distributions of noble gas spectral lines, in both cases a special attention was paid to lines of N_2^+ and N_2. The obtained mapping of the plasma jet shows very different number density distributions of relevant excited species. In the case of helium plasma jet, strong N_2^+ lines were observed. In contrast to that, the intensities of N_2 lines in Ar were below the present detection limit. The positions of N_2^+ and N_2 distribution maxima in helium indicate the regions where the highest efficiency of the water ionization and the protonation process is expected.

© 2011 Elsevier B.V. All rights reserved.

1. Introduction

The coupling of liquid chromatography and mass spectrometry (LC/MS) has been established as one of the most powerful tools in analytical chemistry, especially in biomedical and biochemical analyses, and has resulted in important advances. This is the result of extensive basic research on atmospheric pressure ionization (API) techniques, which offer a robust way to couple LC to MS. The main API techniques are electrospray ionization (ESI) [1,2] atmospheric pressure chemical ionization (APCI) [3–5] and less frequently applied atmospheric pressure photoionization (APPI) [6,7]. ESI, APCI, and APPI differ in their ionization process and their applicability [8].

ESI revolutionized biochemical research by offering a highly sensitive method for the analysis of large biomolecules [9]. It has been widely used also for smaller polar organic molecules, and it is the most popular API technique today. The ionization in an ESI interface is considered primarily as liquid-phase ionization technique: ions formed in a solution are desorbed or evaporated to the gas phase and can subsequently be mass analyzed. The ionization efficiency tends to be poor for more nonpolar compounds. For these, APCI and APPI are more suitable.

The ionization conditions in APCI are considered to be somewhat "harder" than those in ESI [10]. The ionization in APCI is understood to be primarily based on gas-phase ion–molecule reactions between analyte molecules and a solvent-based reagent gas, generated by a series of ion–molecule reactions initiated by electrons from the corona discharge needle.

APPI has been introduced as an alternative ionization technique to APCI-MS for nonpolar compounds, [6,7]. The APPI interface can be considered as a modified APCI source, with the corona discharge being replaced by a gas discharge lamp except that other ionization mechanisms will take place.

In APCI, the initial ionization by corona discharge takes place in a very small volume near the needle tip. Therefore, it can be expected that an increased plasma volume results in a larger fraction of ionized analytes, leading to improved sensitivity.

A dielectric barrier discharge (DBD) can be used to generate low-temperature plasmas at atmospheric pressure [11,12]. The DBD is typically formed between two electrodes, with at least one dielectric layer, which separates the electrode from the plasma. The DBD plasmas are suitable for the atomization of volatile species [13–15]. Furthermore, different geometrical arrangements have also served as an ionization source for ambient MS [16–19] and ion mobility spectrometry (IMS) [20–22]. The miniaturized plasma was found to be a stable and efficient ionization source and was, for this reason, ideal for ion mobility spectrometry.

Furthermore, DBD offers a new approach for efficient ionization for LC/MS applications [23]. A dielectric barrier discharge ionization (DBDI) was implemented into a commercial API interface for LC/MS

* Corresponding author.
E-mail address: joachim.franzke@isas.de (J. Franzke).

applications. A heterogeneous compound library was investigated by DBDI to illustrate the potential use of the miniaturized plasma as an alternative ionization technique to ESI, APCI, and APPI.

As shown in [21], a plasma jet produced by capillary DBD running in helium can be used as very efficient soft ionization source. Here, nitrogen molecules contained in air are recognized to play a crucial role due to interaction with helium metastable atoms in the plasma jet. The energies of helium metastables lie above the ionization limit of N_2, which would then in principle enable the production of excited nitrogen molecules N_2^+ (B $^2\Sigma_u^+$) by Penning ionization. Furthermore, the interaction between nitrogen ions and water molecules in the air leads, in a cascade of processes, to an efficient protonation. In contrast to He, the energies of Ar and Ne metastables are lower than the N_2 ionization limit, and the Penning ionization is not expected to be efficient. Indeed, as reported in [21], the interaction between Ar or Ne plasma jet and air yielded no measurable N_2^+ ion signals. In addition, very small protonation effects in the case of neon were observed, while in the case of argon these effects could not be detected.

The dissociation process of water by collisions of N_2^+ and the protonation process of sample molecules should spatially be in the vicinity of the maximum N_2^+ population. Therefore, a spatially resolved measurement of the soft ionization plasma jet is of special interest. In the present work 2D spatially resolved optical emission measurements of capillary DBD plasma jets burning in He as well as in Ar were performed. The obtained line intensity distributions correspond to the position-dependent number densities of relevant excited species, i.e. excited noble gas atoms, N_2^+ and N_2. These distributions are clearly different and indicate the region in the plasma jet where the protonation process can occur.

2. Experiment and measurements

2.1. Experimental arrangement for the helium plasma jet mapping

In the present work the plasma jet is generated by a dielectric barrier discharge (Fig. 1). The DBD is constructed using a 30 mm long glass capillary having an outer diameter of 1.2 mm and an inner diameter of 0.5 mm. One end of the capillary is the gas inlet and the

other end is left in open air. Two copper disc shaped electrodes with a thickness of 1 mm and a central orifice are mounted on the capillary at a distance of 10 mm one to the other. The orifices of the electrodes have the same diameter as the outer capillary diameter, so they are as tight as possible on the glass to provide a good connectivity between them and the dielectric glass. The electrodes are encapsulated in Teflon plates to prevent direct arc discharges between them. The distance from the open end of the capillary to the first electrode (the anode) is approximately 2 mm. The whole construction – capillary, electrodes and connecting cables – is encapsulated in a Teflon cage.

The plasma jet is obtained using He as working gas which is provided with two different gas flow-rates $F_A = 300$ and $F_B = 1000$ ml min^{-1}. The electrodes are connected through isolated cables to a home built high voltage generator [25]. A function generator that provides rectangular pulses of 2 µs width modulates the signal applied on the electrodes. The corresponding values for stable plasma are 6 kV at 20 kHz.

Depending on the gas flow-rate the plasma jet has lengths of 10 and 20 mm for the 300 and 1000 ml min^{-1}, respectively.

The plasma jet mapping was performed by optical emission spectroscopy. For this purpose an USB4000 spectrometer in the visible range (300–956 nm) and an optical fiber 600 µm UV/VIS 300–1100 nm from Ocean Optics were used together with OOIBase32 software. The optical arrangement applied for plasma jet mapping is presented schematically in Fig. 1. The top view of the plasma jet, the focusing lens (f = 10 mm) and the entrance of the optical fiber are depicted in the upper part. The lower part shows a vertical section of the arrangement. Both the Teflon cage encapsulating the glass capillary and the acquiring end of the optical fiber are mounted on micrometric stages that allow three-dimensional adjustments. These parts are adjusted by means of a He–Ne laser to be on the same optical axis (y-axis, not shown in the figure). The distances between the plasma jet and the lens and between the lens and the optical fiber determine an object to image ratio of 1:2. Since the aperture of the optical fiber was about 0.5 mm, only the light from a thin column along the optical axis of the investigated plasma jet was detected.

The effective jet mapping was performed by translating the capillary along the x-axis in 1 mm steps. For each x position the optical fiber was shifted along the vertical axis (z) in 0.1 mm steps
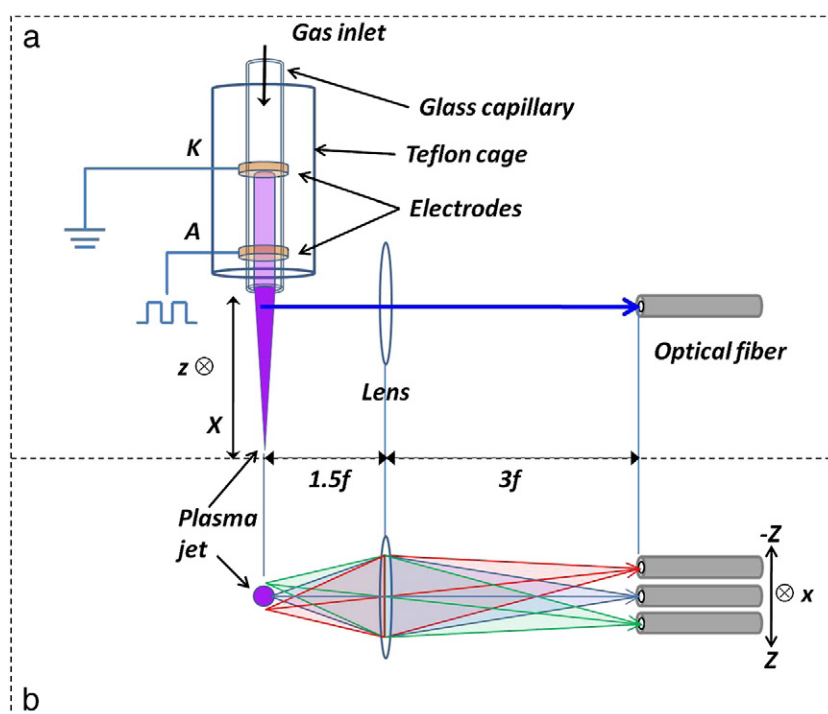

Fig. 1. Optical arrangement for plasma jet mapping: a) top view, b) section view (end-on).

symmetrically with respect to the x-axis. Thus, the different parts of the jet were imaged on the optical fiber with spatial discrimination in z-direction of 0.5 mm (optical fiber diameter). At each (x, z) position the spectra were acquired with 500 ms integration time. The spectra were taken at five and nine x-positions, for lower and higher gas flow-rates, respectively. The spectra were stored by a laboratory PC for further analysis.

2.2. Measurements and results obtained for the helium plasma jet

Some results of the plasma jet mapping obtained at lower flow-rate of helium (flow-rate $F_A = 300$ ml min^{-1}) are illustrated in Fig. 2. In that figure the intensities of two spectral lines for each of He, N_2^+, and N_2 are shown starting at the x_1 position, which is at 1 mm away from the orifice of the capillary. The spectral line peak intensities measured at particular (x, z) positions are represented by contours of constant intensity. Areas between the contours are filled with shades of gray in the range between white (intensity maxima) and black. There is a clear difference between the spatial intensity distributions of each type of the emitting species. Helium lines exhibit intensity maximum close to the capillary orifice, where the intensities of the N_2^+, and N_2 lines are very weak. At a distance of about 2 mm from the capillary orifice both the N_2^+ and the N_2 line groups reach their maxima. With further increase of distance x, intensities of the N_2^+ lines decrease faster than the intensities of the N_2 lines.

When a higher helium flow-rate of 1000 ml min^{-1} (F_B) is applied through the capillary barrier discharge, the general picture remains the same as given in Fig. 2. However, the regions of the N_2^+, and the N_2 line intensity maxima are shifted further away from the capillary end. In addition, the intensity distributions are broader along the x-axis than for the lower He flow-rate. This effect is illustrated in Fig. 3.

A quantitative description of investigated spatial line intensity distributions is given in Fig. 4, where a part of the data set from Fig. 3 is extracted. The plasma jet is radially nearly symmetric with respect to the x-axis. Due to the fact that the glass capillary could not be perfectly horizontally arranged the plasma jet had a small inclination, which could be the reason for a slight asymmetry. However, as one can see in Fig. 4 (left), the radial intensity distributions of the He, N_2^+, and N lines, i.e. the intensities measured along the z-axis cannot be distinguished within the error bars. These distributions are governed by diffusion of excited helium atoms into surrounding atmosphere in radial direction. However, as already shown in Figs. 2 and 3, the distributions of the species mentioned earlier are strongly separated in the x-direction, which is governed by the helium flow-rate. The data in Fig. 4 (right) are presented in semi-logarithmic plot, where the linear fits for the largest distances indicate that all three distributions exhibit exponential decrease. In contrast to the He and N_2^+ lines, the N_2 line intensities decrease much slower.

The intensity of an optically thin spectral line is proportional to the product of the number density in the relevant upper state and the
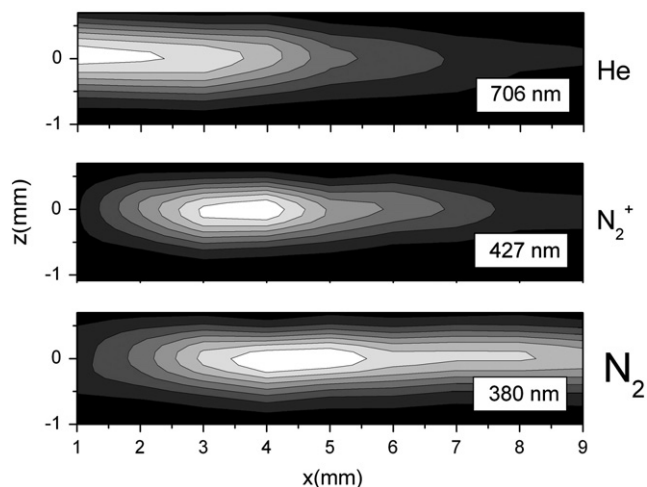

Fig. 3. Two-dimensional contour plot of intensity distributions in z–x plane for He 706 nm line (upper part), N_2^+ 427 nm line (middle part) and N_2 380 nm (lower part). White areas indicate the regions of intensity maxima. The measurements were performed the He flow-rate $F_B = 1000$ ml min^{-1}.

corresponding radiative transition probability. Thus, spatial intensity distributions of optically thin lines emitted by different species yield the information about position-dependent relationships between number densities in relevant upper states.

2.3. Comparison between He and Ar plasma jets.

Another set of similar measurements was carried out in order to get a comparison between He and Ar. The same dielectric barrier capillary plasma jet discharge was used in the same electrode configuration and polarization and with the same ignition and sustaining voltage characteristics. The noble gas flows used were 500 ml min^{-1} and 100 ml min^{-1}, for helium and argon, respectively. The applied argon flow was a maximum flow at which the argon plasma jet could still be sustained. To make a better comparison between He and Ar measurements the jets should be nearly of the same length and intensity, so that approximately the same amount of nitrogen from air would diffuse into the plasma jet and be excited or ionized by the reactive particles of the plasma. This requirement was fulfilled with He flow applied here.

The results are presented in Fig. 5. In the case of the He plasma jet the shapes of the investigated intensity distributions along the x-axis are qualitatively similar to the previously obtained ones. The intensity of the He 706 nm line exhibits a maximum at the capillary exit, and with increasing x-position the maxima of N_2^+ and N_2 line intensities appear. The positions of the maxima of N_2^+ and N_2 are in accordance with the results presented in Section 2.2. The maxima shown in Fig. 5 have a
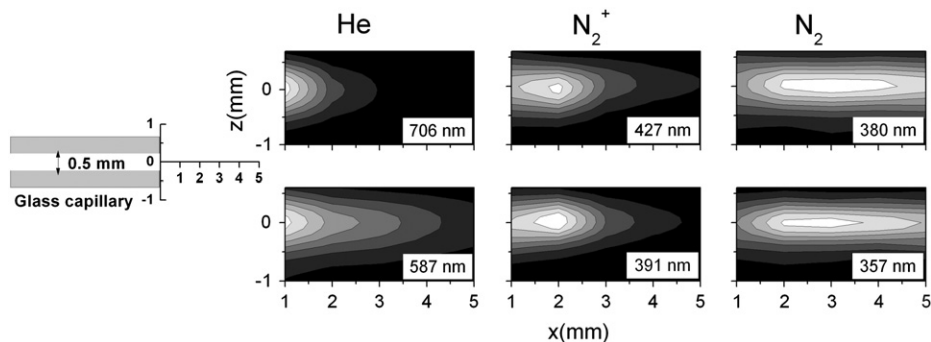

Fig. 2. Spatial intensity distributions of two He, N_2^+, and N_2 lines represented in / two-dimensional contour plot. White areas indicate the regions of maximum intensity in the z–x plane. The measurements were performed at the flow-rate $F_A = 300$ ml min^{-1} through the capillary.
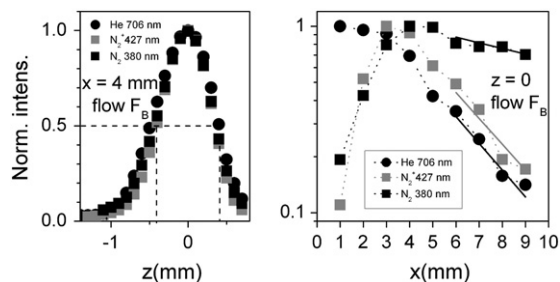
Fig. 4. Intensity distributions of the He 706 nm, the N_2^+ 427 and the N_2 380 lines extracted from the data presented in Fig. 3. Left: Normalized radial line intensity distributions represented by measurements along the z-axis at the position x = 4 mm. Full width at half-maximum of radial intensity distributions amounts to about 0.9 mm. Right: Normalized intensity distributions along the x-axis (z = 0) presented in semi-logarithmic plot. The size of used symbols approximately represents the experimental error bars. Full straight lines are linear fits through data at the four largest values of x.

slightly stronger shift than obtained with the flow $F_A = 300$ ml min^{-1}, but less than that in the case of $F_B = 1000$ ml min^{-1}.

In case of the argon plasma jet, only the emission line of N_2 could be observed (represented here by the N_2 357 nm line) while the emission intensity of N_2^+ lines could not be detected.

The normalized intensities along the x-axis for z = 0 for the investigated emission lines in case of He as well as in case of Ar are presented in semi-logarithmic plot in Fig. 6. As one can see from that picture, the He 706 nm line as well as the Ar 912 nm line exhibit nearly exponential decrease, where the slope for Ar is higher than for He. The intensity distributions of the N_2 357 nm line show maxima in both He and Ar cases. These distributions decrease slower than the corresponding noble gas line intensities.

Intensity distributions along the z-axis (representing the radial distributions) of the investigated lines in both plasma jets are presented in Fig. 7. The positions chosen are x = 3 mm for the He plasma, and x = 2 mm for the Ar plasma. At these x-positions, the corresponding N_2 357 nm line intensity distributions exhibit their maxima.

3. Possible excitation and de-excitation paths

In the present experiment, several He lines (at 501, 587, 667, 706 and 728 nm) have been observed. They correspond to the transitions from higher excited states to either 2p $^1P^o$ resonance state or the lower-lying 2p $^3P^o$ and 2s ^1S states. The latter is one of the two helium

metastable states. As for the He 706 nm emission line, it emerges in the 3s $^3S_1 \rightarrow$ 2p $^3P^o$ transition with the energies of the higher and the lower level equal to 22.72 eV and 20.96 eV, respectively.

The argon spectra exhibit intense emission lines in the wavelength range of 700 nm–950 nm. These lines are assigned to the transitions from $2p_{1-10}$ states (energies: between 12.09 eV and 13.48 eV) to the $1s_{2-4}$ metastable state as well as to the $1s_5$ resonance state (energies: between 1.55 eV and 11.83 eV).

The excitation of higher lying noble gas states is due to impact with fast electrons that are accelerated inside the capillary in the regions near the electrodes. The radial symmetry of the electrodes produce the so-called "hollow cathode effect" that increases the collision rate between the kinetic electrons and gas atoms increasing the densities of reactive species (excited atoms and ions).

In our previous paper [22], the paths leading to the population of relevant excited states have been proposed. The N_2 357 nm emission lines correspond to the following transition N_2 (C $^3\Pi_u^+$) $\rightarrow N_2$ (B $^3\Pi_g^+$) [24]. The N_2 (C $^3\Pi^+$) state can be populated in several ways. First, it can be populated through the direct electron impact excitation from the N_2 ground state: N_2 (X $^1\Sigma_g^+$)$_{v=0}$ + e $_{fast} \rightarrow N_2$ (C $^3\Pi_u^+$)$_{v=0,1}$ + e $_{slow}$, where the threshold energy of fast electrons equals to 11.1 eV. In this case, the population rate for the upper level of the N_2 357 nm transition is proportional to the N_2 ground state number density and the density of fast electrons. A second possible population mechanism of the N_2 (C $^3\Pi_u^+$) state is through electron recombination of the N_2^+ (X $^2\Sigma_g^+$) followed by decay. When argon is used as working gas, a third possibility to populate the N_2 (C $^3\Pi_u^+$) arises. This is represented by energy transfer due to collision between N_2 (B $^3\Pi_g^+$) state and Ar metastable state that has the energy level just above the N_2 (C $^3\Pi_u^+$) state as represented in Fig. 8.

The N_2^+ 391 nm and 427 nm emission lines correspond to the transition (B $^2\Sigma_u^+$) $\rightarrow N_2^+$ (X $^2\Sigma_g^+$) and they cannot be initiated in pure nitrogen plasmas at atmospheric air [24]. The population of the N_2^+ (B $^2\Sigma_u^+$) level is possible through two different processes. The first one is the one-step electron impact ionization process: N_2 (X $^1\Sigma_g^+$)$_{v=0}$ + e$^-$ (E>18.7 eV) $\rightarrow N_2^+$(B $^2\Sigma_u^+$)$_{v=0}$ + 2e$^-$. The second one is the two-step process: N_2 (X $^1\Sigma_g^+$)$_{v=0}$ + e$^-$ (E>15.5 eV) $\rightarrow N_2^+$ (X $^2\Sigma_g^+$)$_{v=0}$ + 2e$^-$ followed by: N_2^+ (X $^2\Sigma_g^+$)$_{v=0}$ + e$^-$ (E>3.2 eV) $\rightarrow N_2^+$ (B $^2\Sigma_u^+$)$_{v=0}$ + e$^-$. These processes take place probably during the initial increase and the early decay of the current pulse when the density of fast electrons inside the capillary is high. However, one should keep in mind that the DBD burns in a relatively short period of time (in the present experiment less than 2 µs) and in the relatively long period of time between two discharge pulses (about 100 µs) there are no fast electrons present.
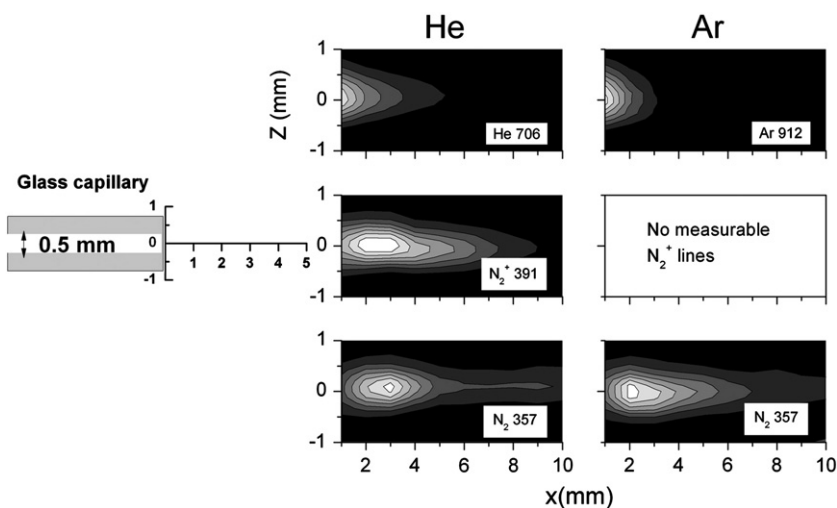

Fig. 5. Spatial intensity distributions of He, N_2^+, and N_2 measured in the He plasma jet in comparison with Ar and N_2 lines measured in the Ar plasma jet represented in two-dimensional contour plot. White areas indicate the regions of maximum intensity in the z–x plane. The measurements were performed at the flow-rate $F_C = 500$ ml min^{-1} for He and $F_D = 100$ ml min^{-1} for Ar through the capillary.
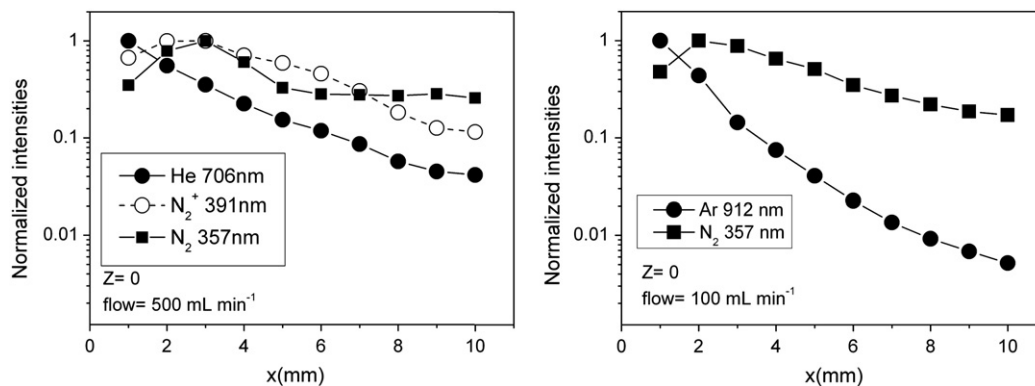
Fig. 6. Normalized intensity distributions along the x-axis (z = 0) presented in semi-logarithmic plot for the He 706 nm, N_2^+ 391 and N_2 357 nm on the left side, and Ar 912 nm and N_2 357 nm lines on the right side. Data are extracted from the results presented in Fig. 5. The size of used symbols approximately represents the experimental error bars.
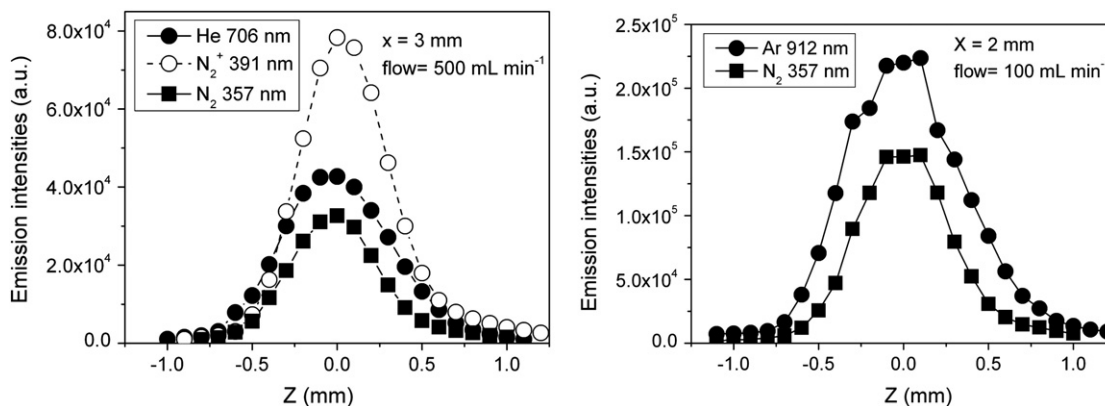

Fig. 7. Radial intensity distribution of the investigated emission lines: left He jet (357 nm, 391 nm and 706 nm), right Ar jet (357 nm and 912 nm).

Nevertheless, as shown by time-resolved measurements reported by Xiong et al. [26], the excited N_2^+ are present in this "dark" period between two discharge pulses when plasma is generated in helium. As pointed out in that work, this is most probably due to Penning ionization involving the helium metastables: $He_m + N_2\ (X\ ^1\Sigma_g^+) \rightarrow N_2^+\ (B\ ^2\Sigma_u^+) + He + e^-$. It was shown that the decay of the measured N_2^+ 391 nm line intensity depends on the position at the jet axis. Generally, this decay is much slower than the natural radiative decay and obviously reflects a decay of the source that is responsible for the population of the N_2^+

Fig. 8. Simplified term schemes of He, Ar, N_2 and N_2^+ related to the investigated emission lines (black arrows) and the proposed collisional excitation energy transfers (gray arrows). The ground states of helium and argon ions are labeled with He^+ and Ar^+. For the sake of picture simplicity, relevant excited states of involved particles are represented as single states: He^* — higher excited helium states; He^M — helium metastable states; Ar^* — higher excited argon states; Ar^M — argon metastable states.

$(B\ ^2\Sigma_u^+)$. Most probable sources for this population are the helium metastable atoms. The helium metastables are created in the short pulse periods and their effective lifetime in the later phases is governed by collisions with air components. Here, an additional experimental fact should be considered too. Namely, in the present experiment the measured line intensities at certain position are related to the integral of transient signals. As one can take from Ref. [26], the integrated transient signals of the helium lines are related to the hot plasma bullets, i.e. to the short discharge pulses. In contrast to that, the integrated transient signals related to N_2^+ 391 nm line are mainly due to contributions from the "dark" phase, i.e. from the medium with no fast electrons.

The previously schematically described transition from He_m to N_2^+ $(B\ ^2\Sigma_u^+)$ in collisions with ground state nitrogen molecules is almost resonant and exothermic. Therefore, this reaction is much more probable than the analogous reaction in Ar where the energy of the argon metastables is significantly lower than the energy of the N_2^+ $(B\ ^2\Sigma_u^+)$. The absence of any detectable emission line of N_2^+ when Ar is used as working gas to produce the plasma jet, can be taken as a support for the assumption of the relevant role played by the He metastable in the production of N_2^+ excited.

As pointed out by Xiong et al. [26], another reaction that can lead to the production of N_2^+ $(B\ ^2\Sigma_u^+)$ is represented by the charge transfer reaction as follows: $He_2^+ + N_2 \rightarrow 2He + N_2^+\ (B\ ^2\Sigma_u^+)$. In the opinion of the authors, however, in DBD plasmas generated in mixtures of helium and nitrogen this reaction may not be important in the decay phase during which the positive ions are mostly represented by N_2^+ or N_4^+ but not by the He_2^+.
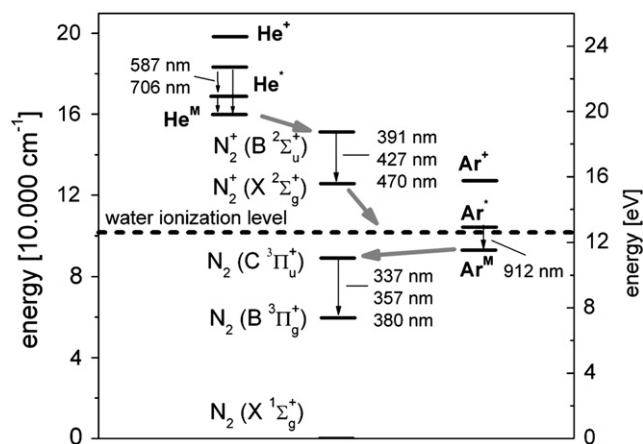
4. Conclusions

The performed spatially resolved spectroscopic measurements on a dielectric barrier discharge plasma jet confirmed results of previous

investigations, while providing additional insight into the relevant excitation energy processes leading to the pronounced ionization of water in air and the subsequent protonation of organic molecules for soft ionization.

Intensity distributions in the plasma jet of some relevant emission lines of the species involved in the energy transfer process (He 706 nm, N_2 380 nm and N_2^+ 427 nm) for three different helium flows (300, 500 and 1000 ml min^{-1}) have been presented. In addition, the analogous measurement was performed with the argon plasma jet for one gas flow (100 ml min^{-1}). The plasma jet, which penetrates from the zone of the capillary barrier discharge into the atmosphere, has strongly non-homogeneous distributions of the ground-state particles. However, the jet is axially symmetric and its non-homogeneity along the axis of penetration is well defined.

By combining the present experimental findings with time-resolved measurements on a helium DBD plasma jet reported by Xiong et al. [26], it can be argued that the main excitation path leading to protonation of water in helium plasma jet penetrating in the air atmosphere starts with the collisions of helium metastables and nitrogen molecules in the air. As a result, we share the opinion of Xiong et al. [26] that Penning ionization of nitrogen molecules and subsequent energy transfer to the water molecules are the processes leading to an efficient water ionization and protonation. In contrast to that, Penning ionization of nitrogen molecules in argon DBD plasma is orders of magnitude less probable than in helium, which can explain no efficient water protonation when argon plasma at similar conditions is used.

Acknowledgement

References

[1] M. Dole, L.L. Mack, R.L. Hines, R.C. Mobley, L.D. Ferguson, M.B. Alice, Molecular beams of macroions, J. Chem. Phys. 49 (1968) 2240–2249.

[2] M. Yamashita, J.B. Fenn, Electrospray ion source. Another variation on the free-jet theme, J. Phys. Chem. 88 (20) (1984) 4451–4459.

[3] E.C. Horning, M.G. Horning, D.I. Carroll, I. Dzidic, R.N. Stillwell, New picogram detection system based on a mass spectrometer with an external ionization source at atmospheric pressure, Anal. Chem. 45 (1973) 936–943.

[4] E.C. Horning, D.I. Carroll, I. Dzidic, M.G. Haegele, M.G. Horning, R.N. Stillwell, Atmospheric pressure ionization (API) mass spectrometry, J. Chromatogr. Sci. 12 (1974) 725–729.

[5] F.J. Andrade, J.T. Shelley, W.C. Wetzel, M.R. Webb, G. Gamez, S.J. Ray, G.M. Hieftje, Atmospheric pressure chemical ionization source. 1. Ionization of compounds in the gas phase, Anal. Chem. 80 (2008) 2646–2653.

[6] D.B. Robb, T.R. Covey, A.P. Bruins, Atmospheric pressure photoionization: an ionization method for liquid chromatography−mass spectrometry, Anal. Chem. 72 (15) (2000) 3653–3659.

[7] J.A. Syage, M.D. Evans, K.A. Hanold, Photoionization mass spectrometry, Am. Lab. 32 (24) (2000) 24–29.

[8] W.M.A. Niessen, Liquid Chromatography-Mass Spectrometry, 3rd ed.CRC Press, Boca Raton, FL, 2006.

[9] M. Mann, C.K. Meng, J.B. Fenn, Interpreting mass spectra of multiply charged ions, Anal. Chem. 61 (15) (1989) 1702–1708.

[10] W.M.A. Niessen, State-of-the-art in liquid chromatography–mass spectrometry, J. Chromatogr. A 856 (1999) 179–197.

[11] M. Miclea, K. Kunze, G. Musa, J. Franzke, K. Niemax, The dielectric barrier discharge — a powerful microchip plasma for diode laser spectrometry, Spectrochim. Acta Part B 56 (2001) 37–43.

[12] H.R. Snyder, G.K. Anderson, Effect of air and oxygen content on the dielectric barrier discharge decomposition of chlorobenzene, IEEE Trans. Plasma Sci. 26 (1998) 1695–1699.

[13] Z. Zhu, S. Zhang, Y. Lv, X. Zhang, Atomization of hydride with a low-temperature atmospheric pressure dielectric barrier discharge and its application to arsenic speciation with atomic absorption spectrometry, Anal. Chem. 78 (2006) 865–872.

[14] Y.-L. Yu, Z. Du, M.-L. Chen, J.-H. Wang, A miniature lab-on-valve atomic fluorescence spectrometer integrating a dielectric barrier discharge atomizer demonstrated for arsenic analysis, J. Anal. At. Spectrom. 23 (2008) 493–499.

[15] Z. Zhu, J. Liu, S. Zhang, X. Na, X. Zhang, Determination of Se, Pb, and Sb by atomic fluorescence spectrometry using a new flameless, dielectric barrier discharge atomizer, Spectrochim. Acta Part B 63 (2008) 431–436.

[16] N. Na, M. Zhao, S. Zhang, C. Yang, X. Zhang, Development of a dielectric barrier discharge ion source for ambient mass spectrometry, J. Am. Soc. Mass Spectrom. 18 (2007) 1859–1862.

[17] N. Na, C. Zhang, M. Zhao, S. Zhang, C. Yang, X. Fang, X. Zhang, Direct detection of explosives on solid surfaces by mass spectrometry with an ambient ion source based on dielectric barrier discharge, J. Mass Spectrom. 42 (2007) 1079–1085.

[18] Y. Zhang, X. Ma, S. Zhang, C. Yang, Z. Ouyang, X. Zhang, Direct detection of explosives on solid surfaces by low temperature plasma desorption mass spectrometry, Analyst 134 (2009) 176–181.

[19] X. Ma, S. Zhang, Z. Lin, Y. Liu, Z. Xing, C. Yang, X. Zhang, Real-time monitoring of chemical reactions by mass spectrometry utilizing a low-temperature plasma probe, Analyst 134 (2009) 1863–1867.

[20] A. Michels, S. Tombrink, W. Vautz, M. Miclea, J. Franzke, Spectroscopic characterization of a microplasma used as ionization source for ion mobility spectrometry, Spectrochim. Acta Part B 62 (2007) 1208–1215.

[21] W. Vautz, A. Michels, J. Franzke, Micro-plasma: a novel ionisation source for ion mobility spectrometry, Anal. Bioanal. Chem. 391 (2008) 2609–2615.

[22] S.-B. Olenici-Craciunescu, A. Michels, C. Meyer, R. Heming, S. Tombrink, J. Franzke, Characterisation of a capillary dielectric barrier plasma jet for use as a soft ionization source by optical emissions and ion mobility spectrometry, Spectrochim. Acta Part B 64 (2009) 1253–1258.

[23] H. Hayen, A. Michels, J. Franzke, Dielectric barrier discharge ionization for liquid chromatography/mass spectrometry, Anal. Chem. 81 (24) (2009) 10239–10245.

[24] A. Qayyum, Y. Shaista, A. Naveed, S.A. Ghauri, M. Zakaullah, Diagnostics of nitrogen plasma by trace rare-gas–optical emission spectroscopy, J. Appl. Phys. 98 (2005) 103303-1–103303-9.

[25] R. Heming, A. Michels, S.B. Olenici, S. Tombrink, J. Franzke, Electrical generators driving microhollow and dielectric barrier discharges applied for analytical chemistry, Anal. Bioanal. Chem. 395 (2009) 611–618.

[26] Q. Xiong, X. Lu, J. Liu, Y. Xian, Z. Xiong, F. Zou, C. Zou, W. Gong, J. Hu, K. Chen, X. Pei, Z. Jiang, Y. Pan, Temporal and spatial resolved optical emission behaviours of a cold atmospheric pressure plasma jet, J. Appl. Phys. 106 (2009) 083302-1–083302-6.